

Ship-track-based assessments overestimate the cooling effect of anthropogenic aerosol*

Franziska Glassmeier,^{1,2,3*} Fabian Hoffmann,^{3,4} Jill S. Johnson,⁵
Takanobu Yamaguchi,^{3,4} Ken S. Carslaw,⁵ Graham Feingold⁴

¹Department Geoscience and Remote Sensing, Delft University of Technology, Netherlands

²Department of Environmental Sciences, Wageningen University, Netherlands

³Cooperative Institute for Research in Environmental Sciences, University of Colorado, USA

⁴NOAA Chemical Sciences Laboratory, Boulder, USA

⁵School of Earth and Environment, University of Leeds, UK

*Correspondence: f.glassmeier@tudelft.nl

Abstract

The effect of anthropogenic aerosol on the reflectivity of stratocumulus cloud decks through changes in cloud amount is a major uncertainty in climate projections. The focus of this study is the frequently occurring non-precipitating stratocumulus. In this regime, cloud amount can decrease through aerosol-enhanced cloud-top mixing. The climatological relevance of this effect is debated because ship exhaust does not appear to generate significant change in the amount of these clouds. Through a novel analysis of detailed numerical simulations in comparison to satellite data, we show that results from ship-track studies cannot be generalized to estimate the climatological forcing of anthropogenic aerosol. We specifically find that the ship-track-derived sensitivity of the radiative effect of non-precipitating stratocumulus to aerosol overestimates their cooling effect by up to 200%. This offsetting warming effect needs to be taken into account if we are to constrain the aerosol-cloud radiative forcing of stratocumulus.

*This preprint is intended for publication in a scientific journal but has not been peer-reviewed. The copyright is maintained by the authors or by other copyright owners. It is understood that all persons copying this information will adhere to the terms and constraints invoked by this copyright.

Introduction

Clouds interact with radiation and therefore play an important role in the planetary energy balance. Their net effect is to cool the planet by reflecting incoming short-wave radiation [1]. Covering large parts of the sub-tropical oceans, stratocumulus (Sc) clouds are by far the largest contributor to this cooling [2]. Anthropogenic perturbations to cloud reflectivity that result from an increased concentration of atmospheric aerosol particles are the most uncertain anthropogenic forcing of the climate system [3, 4]. As a striking illustration of this effect, exhaust from ships can create “ship tracks” that manifest as bright linear features in Sc decks. This brightening arises because exhaust-aerosol particles form the nuclei of cloud droplets. A greater abundance of particles means that a cloud consists of more, but smaller droplets, which enhances the radiant energy reflected to space [5]. Changes in the number and size of cloud droplets also influence cloud physical processes [6–11]; for the example of ship tracks this means that the amount of cloud water inside and outside of a track may evolve differently. Globally, the large uncertainty in the cloud-mediated aerosol forcing arises from the unknown magnitude of such *adjustments* of cloud water in response to aerosol-induced perturbations [3, 12, 13]. Here we show that despite providing a striking illustration of aerosol-cloud interactions, ship tracks *do not* provide suitable data to estimate the magnitude of cloud liquid-water adjustments in a polluted climate, in contrast with the common assumption that ship tracks *do* represent such adjustments [14–17].

In non-precipitating Sc, cloud response to aerosol perturbations is commonly quantified by the sensitivity [4, 18, 19]

$$S = \frac{dA_c}{dN} = \frac{A_c(1 - A_c)}{3N} \left(1 + \frac{5}{2} \frac{d \ln \text{LWP}}{d \ln N} \right) \quad (1)$$

of cloud albedo A_c to cloud droplet number N . The first term on the right-hand side of Equation 1 quantifies the albedo effect of changing droplet number when keeping the vertically integrated amount of liquid water, or *liquid-water path*, LWP, constant; the second term accounts for cloud water adjustments as quantified by the relative sensitivity $d \ln \text{LWP} / d \ln N$ of LWP to N . Numerical values for LWP-adjustments $d \ln \text{LWP} / d \ln N$ have been derived from detailed modeling and satellite studies [8, 14–17, 20–26]. Both approaches have recently converged on the insight that the sign of LWP adjustments is regime-dependent (Figure 1). Adjustments tend to be positive

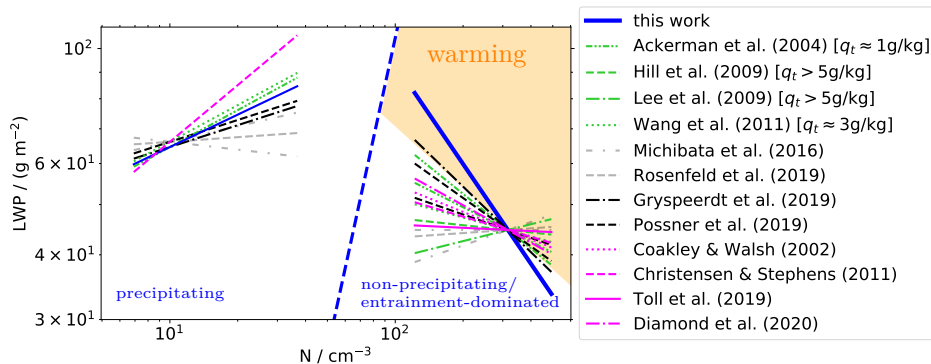


Figure 1: Reported log-log-linear relationships between liquid-water path, LWP, and cloud droplet number, N , in comparison to this work. Lines are based on reported slopes (Table S1), axis intercepts have been added as suitable for illustration. The dashed blue line indicates a critical droplet radius for precipitation formation (based on a mean droplet radius of $12 \mu\text{m}$ at cloud top for an adiabatic condensation rate of $2.5 \cdot 10^{-6} \text{ kg m}^{-4}$), which separates the precipitation-dominated regime on the left from the non-precipitating, entrainment-dominated regime on the right. The latter is the focus of this study. Colors distinguish results from large-eddy simulations (green), climatological satellite studies (black), and satellite studies of ship tracks (magenta). Results in grey are shown for completeness but are not directly comparable due to differences in methodology. For large-eddy simulation studies, above-cloud absolute humidity q_t is indicated. Solid blue lines show values derived in this work (Table S1 and S4, in particular $d \ln \text{LWP} / d \ln N = -0.64$ in the entrainment regime). The orange shading indicates where LWP adjustments are sufficiently negative to lead to climate warming rather than cooling based on the sign of albedo sensitivity S (Equation 1).

under precipitating conditions where the addition of particles decreases drop size, increases colloidal stability, and allows for an accumulation of liquid water [6]. A positive LWP adjustment thus implies thicker, more reflective clouds that have a stronger cooling effect. The effects of aerosol perturbations on precipitation were considered recently [25]. In the current work we focus on non-precipitating Sc whose development is dominated by entrainment. Observations show that this Sc regime is more common than the precipitating regime [26, 27]. Non-precipitating Sc feature negative adjustments, indicating a decrease in LWP for higher aerosol concentrations. The decrease in LWP stems from the accelerated and stronger evaporation of cloud liquid in higher aerosol conditions as the Sc mixes with dry air from above the cloud (*entrainment*). Smaller droplets evaporate more efficiently because they provide a larger surface (for a given total amount of liquid) and reside closer to the entrainment interface than larger droplets due to reduced gravitational settling, which increases the potential for evaporation [7–11, 28]. Negative LWP adjustment values indicate thinner, less reflective clouds and

a weaker cooling effect. When the darkening effect of cloud thinning is stronger than the brightening of increased N , negative LWP adjustments can even imply a warming effect. In non-precipitating Sc, this is the case when $d \ln \text{LWP} / d \ln N < -2/5$ such that Equation 1 becomes negative (orange shading in Figure 1).

In addition to the distinction between the entrainment- and precipitation-dominated regimes, satellite studies have identified above-cloud moisture as an important control on the magnitude of LWP adjustments in Sc [15, 24, 26, 29]. This is consistent with process-understanding from detailed cloud modeling studies (*large-eddy simulation*, LES), where drier above-cloud conditions correspond to a stronger aerosol-effect on entrainment (Figure 1). As another factor behind the variability of adjustment estimates, references [15, 30] discuss the effects of N -LWP *co-variability* that results from large-scale co-variability of aerosol and moisture. As an example of this confounding effect, compare a maritime situation with a clean and moist atmosphere to a polluted and drier continental case. Observations from these two cases will likely show that higher N is correlated with lower LWP [31], suggesting a negative LWP-adjustment. Clearly, the “adjustment” quantified here is not related to the effect of aerosol on cloud properties driven by entrainment or precipitation formation that we seek to capture, but rather, to large-scale conditions.

A special appeal of ship tracks has been that they are not affected by external co-variability because the large-scale meteorological conditions are the same inside and outside of the track. Accordingly, results from targeted satellite analyses of ship-tracks [14, 16, 20] have been assigned higher credibility than climatological satellite studies, for which external co-variability cannot be ruled out. In particular, the comparably large absolute adjustment values found in the latter studies have been attributed to aerosol-moisture co-variability, assuming that weak-to-almost absent LWP adjustments identified by ship-track studies [14, 16, 20] provide the best estimate for LWP adjustment. In contrast to this assumption, a recent study of shipping lanes reports significantly negative adjustment values [17].

In this article, we show that the current emphasis on satellite studies of ship tracks to estimate LWP adjustments leads to an overestimation of the cooling effect of aerosols in Sc. We furthermore reconcile the broad range of reported adjustment estimates and discuss implications of our results for identifying alternatives to ship-track studies. Our argument is illustrated in Figure 2 and builds on two key results: Firstly, LWP adjustments become more negative as Sc decks evolve towards a steady-state, bounded from

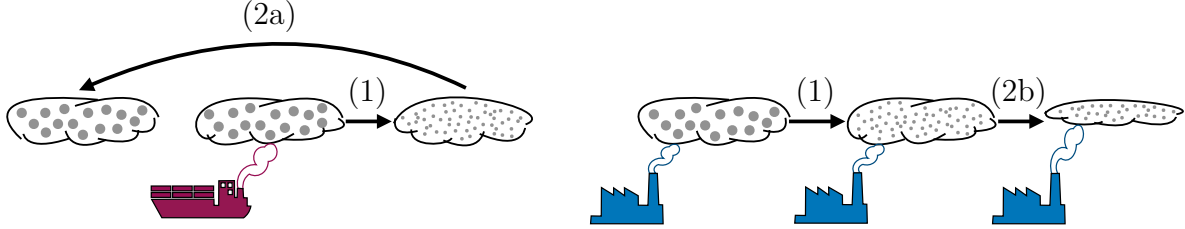


Figure 2: LWP adjustments in ship tracks, which persist for a few hours, as compared to industrial-era pollution, which perturbs the climatological aerosol background and leads to perturbations that last for days. As an initial response to the aerosol perturbation, both situations feature cloud brightening through more but smaller cloud droplets at constant LWP (step 1). The ship track then returns to its original state because the perturbation ceases (step 2a). An enhanced aerosol background, in contrast, persists and allows for LWP to equilibrate to a new steady state that is characterized by increased entrainment efficiency and a lower LWP (step 2b).

below by $d \ln \text{LWP} / d \ln N = -0.64$. Secondly, in ship tracks, this temporal evolution does not proceed long enough to be representative of Sc decks in a polluted climate.

Data and methods

Our analysis builds on relating satellite datasets to LES. We make these two data sources comparable by creating an ensemble of 144 LES runs that resembles the scope of a satellite dataset in that it samples a broad range of LWP and N conditions (Figure 3, *Supplementary Information*, [32, 33]). In contrast to satellite data, we prevent externally-induced N -LWP co-variability by sampling initial conditions of ensemble members in a statistically independent way (*Supplementary Information*, [33]). We furthermore limit externally-induced variability in LWP adjustments by fixing external control parameters of Sc (Table S2). We specifically restrict above-cloud absolute humidity to values $q_t < 2.8 \text{ g/kg}$ with a median value of 0.5 g/kg . This choice of very dry above-cloud conditions allows us to derive a lower bound for LWP adjustments.

We approach our investigation of LWP adjustments to N perturbations by analyzing the temporal co-evolution of LWP and N collectively for all members of the Sc ensemble (Figure 3). In the LWP direction, individual ensemble members collectively evolve towards similar LWPs (along an approximately horizontal line in Figure 3). For these steady-state LWPs, there exists a balance in the contributions of different processes that are source and sink terms for LWP - in particular radiative cooling (source), and entrainment and precipitation drying (sink) [34]. The collective evolution in the N direction is structured around the critical radius for precipitation formation [35]. Pre-

precipitating systems (above the dashed line in Figure 3) contain sufficient drops with radii larger than the critical radius, are colloidally unstable, and feature a rapid reduction in N . For systems with smaller radii (below the dashed line), which are our focus, rain is scant and entrainment dominates.

The individual evolution of Sc cloud fields in the ensemble can be represented as flow vectors $\vec{v} = (d \ln N/dt, d \ln \text{LWP}/dt)^T$ in N -LWP space. *Gaussian-process emulation* allows us to interpolate such flow vectors from our limited number of simulations (Figure 3, a) to obtain the full flow field illustrated in Figure 3 (b) (*Supplementary Information*). This interpolation of the flow field enables us to infer cloud behavior beyond the 12h-duration of our simulations, including the behavior when an LWP *steady state* ($d \ln \text{LWP}/dt = 0$) is reached (blue curve in Figure 3, b). This enables us to systematically quantify the time-dependence of LWP adjustments over timescales longer than the duration of our simulations. The flow field representation also allows us to determine that individual Sc systems equilibrate to their steady-state with a characteristic equilibration time scale of $\tau = 9.6$ h (Figure S3, [36]), in excellent agreement with a theoretical estimate [37]. This timescale informs us about the proximity of an observed Sc system to its steady state.

Effect of cloud field evolution towards steady state on adjustment strength

Following the methodology of climatological satellite studies, we derive LWP adjustments $d \ln \text{LWP}/d \ln N$ as slopes of linear regression lines through median LWP values in N -bins. To discuss the time-dependence of adjustments, we separately derive LWP-adjustments per time-step. We illustrate this for $t = 2$ h (magenta data subset in Figure 3, a, and magenta elements in Figure 4, a) and $t = 12$ h (green). Considering all time steps $2 \leq t/h \leq 12$ shows that the LWP adjustment becomes increasingly negative over time (Figure 4, b). This behavior results from the sampling of the N -LWP space by our simulations, which evolves over time. By construction, our dataset initially features an uncorrelated sampling. This explains the almost horizontal regression line and corresponding vanishing adjustment observed at $t = 2$ h. An initial co-variability of N and LWP values would have imprinted an initial correlation and corresponding adjustment value between N and LWP.

As our simulations collectively evolve further from the initial state, they approach the steady-state LWP line (blue curve in Figures 3, 4a) and the sampling of the N -

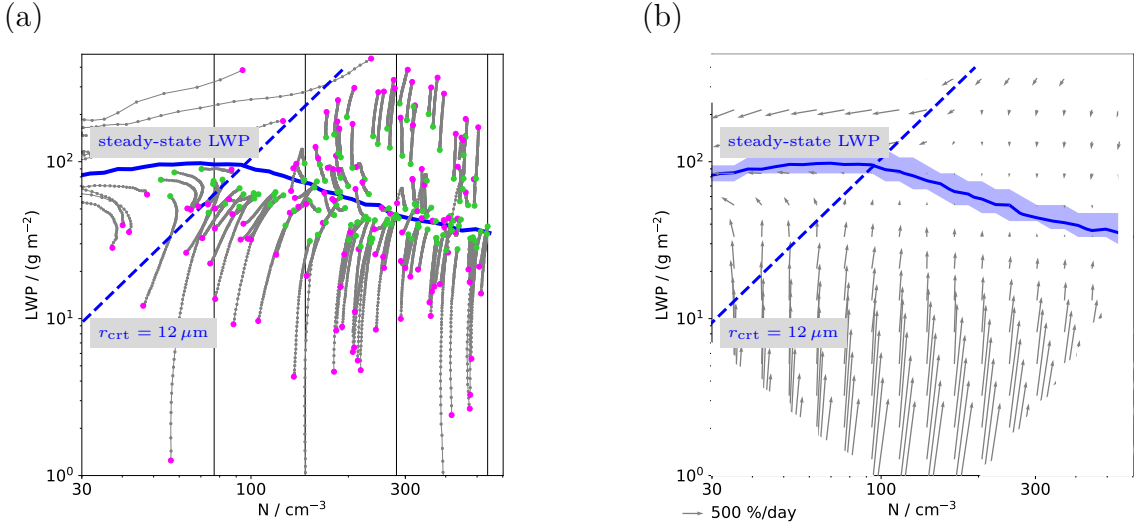


Figure 3: LES ensemble dataset and corresponding temporal co-evolution of liquid-water path LWP and cloud-droplet number N , focusing on the non-precipitating regime below the dashed blue line indicating the critical radius for precipitation formation as in Figure 1. (a) Temporal evolution of 144 LES runs with varying initial conditions. Individual simulation runs are indicated by gray lines connecting gray circles. Start (2 h into the simulation to allow for model spin-up, magenta) and end (12 h, green) of a trajectory are color-highlighted. The solid blue line shows the steady-state LWP from (b). Thin vertical black lines indicate the boundaries of N -bins used in Figure 4. (b) Flow-field representation of LWP- N co-evolution and location of steady-state LWP (blue line and 25th/75th percentile uncertainty shading, Table S4), which is characterized by $d \ln \text{LWP}/dt = 0$.

LWP space features an increasingly negative correlation. Had we run our simulations for longer than 12 h, all ensemble members would eventually have reached their steady-state LWP. This means that for $t \rightarrow \infty$ only the steady-state line is sampled and the LWP adjustment is quantified by the slope of this line. As the slope of the steady-state LWP line reflects the N -dependence of entrainment [34], the LWP-adjustment at $t \rightarrow \infty$, $d \ln \text{LWP}_\infty / d \ln N$, is a direct quantification of N - or more generally aerosol-effects on cloud processes.

For non-precipitating Sc, we obtain $d \ln \text{LWP}_\infty / d \ln N = -0.64$ (Figure 4, a; for uncertainty quantification see Table S4). This value constitutes a lower bound; a more negative adjustment value would require a stronger N -dependent entrainment and therefore drier above-cloud conditions than prescribed for our simulations. This is not realistic since our simulations feature very dry conditions already (Table S2, Figure S4). Figure 1 also supports $-0.64 \leq d \ln \text{LWP} / d \ln N$ as a lower bound on previous

estimates from the literature. We contrast this value with the positive value of the precipitation-dominated branch, for which we determine a slope of 0.21 (Table S4) that lies well within the reported range (Figure 1).

The equilibration of adjustments to the steady-state value is the collective result of the equilibration of individual systems. This allows us to derive that the observed time-dependence of LWP adjustments is accurately described as an exponential decay towards $d \ln \text{LWP}_\infty / d \ln N$ (Figure 4, b),

$$\begin{aligned} \text{adj}(\Delta t) &= \frac{d \ln \text{LWP}_\infty}{d \ln N} \left[1 - \exp\left(-\frac{\Delta t}{\tau_{\text{adj}}}\right) \right], \\ \tau_{\text{adj}} &\approx \tau \left(1 - 1.6 \frac{d \ln \text{LWP}_\infty}{d \ln N} \right) = 2.0 \tau = 20 \text{ h}, \end{aligned} \quad (2)$$

with an adjustment equilibration timescale τ_{adj} that scales with the equilibration timescale of an individual system, τ (Figure S3), and with adjustment strength (*Supplementary Information*). The time-dependence of LWP adjustments on a timescale of almost a day is in stark contrast to the radiative effect of an increased cloud droplet number, which takes full effect in 5 – 10 minutes.

In summary, the extent and interpretation of LWP adjustments in a Sc field depends on the proximity of the system’s LWP to its steady-state LWP. Adjustments based on sampling transient LWP, far from steady state, reflect N -LWP co-variability (or the absence thereof in our case) that is externally prescribed on the system— i.e. a mere *association*; LWP adjustments diagnosed from steady systems reflect aerosol-dependent cloud processes — i.e. a *causal* relationship; intermediate degrees of proximity result in a mixture of both.

Insufficient time for evolution of ship tracks towards steady state

The degree of proximity of an ensemble, or sampling, of Sc systems to its steady-state LWP adjustment can be estimated by comparing the duration of its evolution under an aerosol perturbation, Δt , to the characteristic adjustment equilibration timescale, $\tau_{\text{adj}} = 20 \text{ h}$ (Equation 2). From a Lagrangian perspective, a Sc system is exposed to an aerosol background throughout its lifetime. Typical Sc trajectories in the subtropics persist on timescales of days, $\Delta t_{\text{clim}} > 48 \text{ h}$, before they transition into the shallow cumulus regime due to advection towards higher sea-surface temperatures [38]. Since

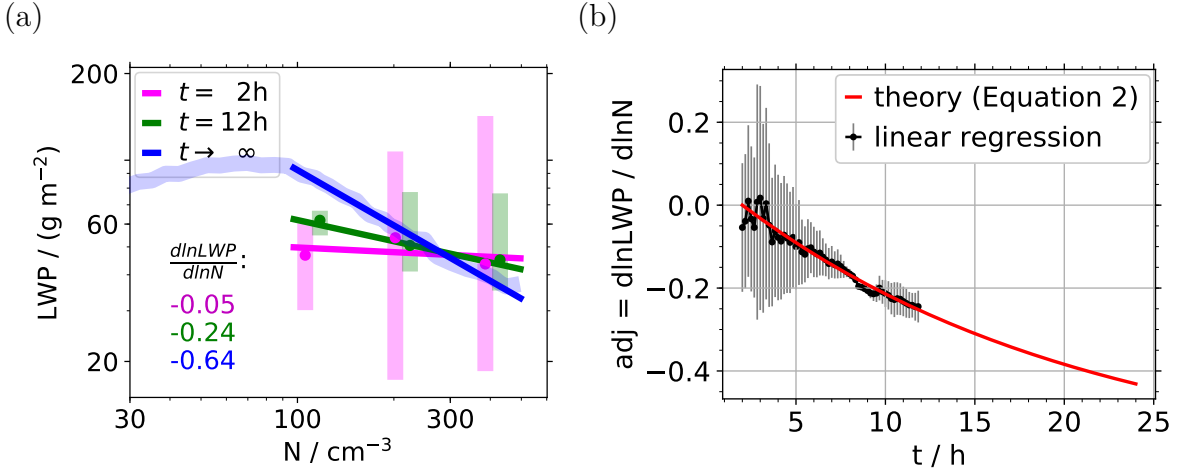


Figure 4: Time-dependence of LWP-adjustments. (a) Data points with error bars show median and 25th/75th percentile of simulated LWP at (magenta) $t = 2$ h and (green) $t = 12$ h for the N -bins indicated in Figure 3 (a). The faint blue curve indicates the steady-state LWP as in Figure 3. Fit slopes $d \ln \text{LWP} / d \ln N$ are indicated. (b) Each data point indicates an adjustment slope obtained as in (a) with error bars for $2 \text{ h} \leq t \leq 12 \text{ h}$. The red line shows the theoretically expected exponential decay (Equation 2).

$\Delta t_{\text{clim}} \gg \tau_{\text{adj}}$, the climatological sampling of Sc is dominated by strongly equilibrated LWPs. While not necessarily composed of steady-state LWPs, we can assume that the LWP climatology of non-precipitating Sc is better characterized as a sampling of steady-state LWPs, than as one of highly transient LWP. Steady-state values as a feasible approximation for Sc properties are in line with previous theoretical studies [39, 40]. A significant probability of Sc being observed close to their steady state is also consistent with relatively narrow climatological distributions of Sc LWPs [15, 41] as transient LWPs are expected to scatter (magenta data in Figure 3, a). A tendency to rapidly re-equilibrate towards a steady state after a perturbation can furthermore explain the observation of resilient, or buffered, cloud behavior [12, 41–43].

Sc decks being strongly adjusted to the aerosol background in which they evolve has implications for constraining the anthropogenic radiative forcing; LWP adjustments need to compare Sc that are strongly adjusted to an aerosol background typical of an industrial-era aerosol climatology (Figure 5, cyan circle at higher N) to Sc decks that are strongly adjusted to a pre-industrial aerosol background (orange circle at lower N). Climatological satellite studies are suitable for this quantification because they predominantly sample strongly-adjusted steady-state LWP. As discussed in the previous

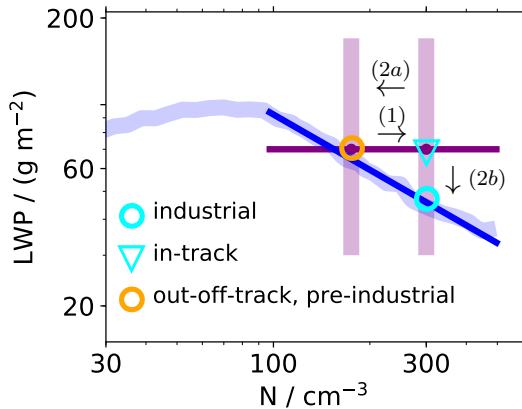


Figure 5: Conceptual illustration of LWP adjustments as derived from ship tracks in comparison to climatological satellite studies in analogy to Figure 4 (a). (Pre-)industrial climatological conditions are strongly-adjusted and represented by circles close to the steady-state (blue line). LWPs within ship tracks are weakly adjusted (triangle symbol) such that ship-track studies are based on comparing almost identical LWP distributions (purple; illustration only, no actual data), which implies vanishing LWP adjustments (purple regression line). Labeled arrows correspond to Figure 2.

section, this specifically means that such studies capture cloud processes, and are only weakly confounded by externally-induced N -LWP co-variability.

Ship-track data are obtained throughout the life of the track, with fresh tracks more likely to be sampled due to their better visibility. With a typical lifetime for ship tracks of 6 – 7 h [44, 45], this corresponds to an average evolution time until sampling of $\Delta t_{\text{ship}} \approx 3$ h. As the characteristic equilibration time exceeds the typical evolution time at sampling, $\Delta t_{\text{ship}} \ll \tau_{\text{adj}}$, we conclude that LWPs sampled from ship tracks are not representative of the aerosol-cloud interaction processes, specifically entrainment, that manifest as a Sc system approaches a steady-state LWP. Instead, their sampling of transient LWPs carries a strong imprint of their specific initial conditions. To characterize these conditions, we describe ship-track studies as a sampling within two different N -bins, one representing out-of-track, and the other in-track conditions (Figure 5). As LWP adjustments are not instantaneous, the LWP distributions within these two bins are identical when the ship exhaust first makes contact with the cloud. As for the idealized initial conditions in our dataset, this corresponds to an initial adjustment of zero (Figure 5, purple regression line). After the perturbation, the in-track distribution evolves to an asymptotic LWP value that is different from that of the out-of-track LWP.

Due to the short duration of this evolution until sampling, adjustment values diagnosed from ship tracks remain small. Indeed, evolution according to Equation 2 corresponds to an adjustment value of

$$\text{adj}(\Delta t_{\text{ship}} = 3 \text{ h}) = -0.1, \quad (3)$$

which matches reported values ranging from -0.2 to 0.0 (Table S1). When, in contrast, sampling a climatologically polluted situation, adjustments can evolve to more negative values before being sampled and values of $\text{adj}(\Delta t_{\text{clim}} = 48 \text{ h}) \approx -0.6$, close to the asymptotic value of -0.64 (Figure 4, a), are obtained.

While ship exhaust may at first glance seem an intriguing proxy for aerosol conditions typical of the industrial-era aerosol climatology, it does not perturb the pristine background for a sufficiently long time (Figure 2). In other words, typical LWPs in ship tracks are not comparable to LWPs in Sc that experience a higher aerosol background due to an anthropogenic shift of the aerosol climatology (Figure 5, cyan circle vs triangle). It needs to be stressed that we only dispute the generalization of LWP adjustments derived from ship track studies to estimate the contribution of LWP adjustments to the overall radiative forcing due to anthropogenic aerosol. Ship tracks do provide reliable estimates of the radiative forcing of the ship tracks themselves.

Implications for the effective radiative forcing due to aerosol-cloud interactions

The discussions in the previous two sections showed that (i) LWP adjustments become more negative as non-precipitating Sc decks evolve under an aerosol perturbation (Figure 4) and (ii) that the LWP in individual ship tracks experiences less time to adjust to the modified aerosol conditions than a Sc deck under climatological high-aerosol conditions (Figure 5). In combination, these two findings imply that ship-track-derived LWP adjustments are less negative than the LWP adjustment that a Sc deck under climatologically polluted conditions exhibits. We contend, therefore, that using ship-track derived adjustment values to estimate the radiative forcing of aerosol-cloud interactions means an underestimation of the absolute effect of LWP adjustments on the radiative forcing. The negative values of LWP adjustments in non-precipitating Sc mean that an increased aerosol load leads to cloud thinning. The associated reduction in short-wave reflectivity implies a warming effect as a result of LWP adjustments that offsets the cooling associated with cloud brightening (Equation 1). Ship-track

studies underestimate this offsetting warming effect of LWP adjustments (Figure 2). With $-0.64 \leq d \ln \text{LWP} / d \ln N$ as lower bound for LWP adjustments (Figure 4), this underestimation corresponds to an overestimation of the cooling effect of aerosols on non-precipitating Sc of up to 200% (*Supplementary Information*). This specifically includes the possibility of an overall warming, rather than cooling, effect of aerosols on non-precipitating Sc (Figure 1). Since non-precipitating Sc occur more frequently than precipitating Sc [26, 27], this warming effect offsets the cooling effect of positive LWP adjustments in precipitating Sc in the overall climate effect of Sc.

For sufficiently strong aerosol perturbations, the aerosol-induced cloud thinning will lead to the complete dissipation of individual clouds in the Sc deck. Such a reduction in cloud fraction through aerosol-enhanced entrainment has previously been reported for a cumulus-under-stratocumulus case [28]. Assuming that cloud properties in steady state are climatologically representative, we estimate that cloud fraction starts to fall below $CF \approx 1$ at $N > 800 \text{ cm}^{-3}$ (Figure S5). Similar cloud fraction adjustments to aerosol perturbations have recently been discussed for the precipitating Sc regime [25, 46]. As for the precipitating case, where cloud fraction adjustments act in the same direction as LWP adjustments (less aerosol leads to more precipitation, less LWP and break-up), aerosol-entrainment-mediated cloud field dissipation enhances the effects of LWP reduction (more aerosol leads to more entrainment, less LWP and reduced cloud fraction). While cloud field break-up due to aerosol-precipitation interactions is observed for low aerosol conditions, cloud field dissipation due to aerosol-entrainment interactions occurs for high aerosol conditions. Cloud fraction adjustments appear particularly relevant under high aerosol conditions because they do not saturate like aerosol effects on cloud albedo (pre-factor $1/N$ in Equation 1, [47]). Aerosol-entrainment induced cloud dissipation therefore implies the possibility of an even more severe underestimation of the warming effect of adjustments by ship-track studies than estimated here.

Our results are consistent with recent satellite estimates of LWP adjustments in Sc [15, 26]. Our insight that the effects of external co-variability fade as a Sc system evolves towards its internal steady-state refutes N -LWP co-variability as the likely explanation for the strongly negative adjustment values reported. This rebuts a main argument invoked to question the results of these studies. At the same time, our modeling results show that strongly negative adjustment values are consistent with existing process understanding. In combination with the limitations of ship-track derived adjustment values discussed above, we therefore conclude that climatological satellite

studies should be assigned more weight for estimating LWP adjustments than ship track studies. Specifically, values of $d \ln \text{LWP} / d \ln N = -0.3$ [26] to -0.4 [15] should be considered possible central values rather than lower bounds as in a recent review [4]. Our analysis establishes the steady-state adjustment $d \ln \text{LWP}_\infty / d \ln N = -0.64$ as a new lower bound for LWP adjustments in non-precipitating Sc.

This recommendation in particular, and our results in general, are moreover consistent with a recent study that derived LWP adjustments from climatological observations of a heavily frequented shipping lane [17]. This setup provides more persistent pollution than an individual ship track, while still suffering from a certain intermittency of pollution as compared to a climatological perturbation. We estimate an effective lifetime of ship tracks in a shipping lane of $\Delta t_{\text{lane}} = 9 \text{ h}$ (*Supplementary Information*). As this time is longer than our estimate for individual ship tracks but shorter than Sc lifetime, it is not surprising that the shipping lane provides a numerical adjustment value that lies in between those derived from single-ship track studies and fully climatological studies (Figure 1). Our results therefore reconcile and explain the differing LWP adjustments that have recently been reported [15–17, 26].

Satellite remote sensing of thin and broken clouds remains a challenge, with large uncertainties in retrieved values [48]. Despite the support for climatological satellite studies that our results provide, it therefore seems desirable to identify alternatives to ship track studies that allow for a direct observation of aerosol effects. Our analysis shows that suitable natural experiments feature temporally continuous pollution. Volcanic emission is an example of a continuously polluting natural experiment, which has so far only been described outside of subtropical Sc regions [16, 49]. As another natural experiment with long-lasting pollution, outflows of polluted continental air over the ocean are also of interest [46]. Lastly, controlled experiments suggested in the context of assessing the feasibility of marine cloud brightening [50] could, by design, provide a sufficiently persistent increase in the aerosol background. At the same time, our results indicate that an intermittent aerosol perturbation, similar to a ship track, may maximize the cooling effect by keeping compensating adjustments small.

In closing, to successfully quantify the cloud-mediated effect of anthropogenic aerosol on the climate system, there is urgent need to quantify the albedo and LWP responses in both precipitating and non-precipitating regions. This will require careful assessment of the frequency of occurrence and areal coverage of these regions, with attendant consideration of the temporal nature of the LWP responses. Estimates of aerosol-cloud

forcing that ignore the non-precipitating regime are likely to significantly overestimate climate cooling.

Supplementary Information

Dataset

This study is based on the ensemble of large-eddy simulations (LESs) described in reference [32]. In comparison to the original dataset, we have excluded outliers in terms of above-cloud humidity, which results in a dataset of 144 LES runs. External, or large-scale, conditions are the same across the LES ensemble and are summarized in Table S2. Variability of LWP within the ensemble is achieved by varying the initial profiles of temperature and moisture; individual simulations vary in N because they have been initialized with varying aerosol backgrounds (Table S3). Following reference [33], we prevent co-variability among the initial conditions by means of a 6D latin-hypercube sampling of the internal factors listed in Table S3. For the derivation of the flow field, additional simulations have been added to achieve a better coverage of the N -LWP space. The dataset and its variants are illustrated in Figure S1.

Derivation of the flow field $\vec{v}(N, \text{LWP})$

The flow field $\vec{v} = (\text{d} \ln N / \text{d}t, \text{d} \ln \text{LWP} / \text{d}t)^T = (v_N, v_{\text{LWP}})^T$ shown in Figure 3 (b) is based on separately deriving the components in the N -direction, v_N , and the LWP-direction, v_{LWP} (Figure S2). To derive these component fields, we first extract tendencies $\text{d} \ln N / \text{d}t$ and $\text{d} \ln \text{LWP} / \text{d}t$ from the data and then interpolate the extracted tendencies by means of *Gaussian-process regression* to obtain emulators for the tendency surfaces.

To derive tendencies, we split each simulated time-series into six intervals of 100 min duration, each of which contains 10 consecutive data points at a 10 min output frequency. For each of these we determine tendencies by fitting trend lines. We only consider significant trends (p-value < 0.05) and assign a value of zero otherwise. To account for oscillatory behavior that occurs because some of our simulations remain influenced by spin-up processes, we assume that the last 100 min-segment of each time-series provides the correct sign of the evolution. The previous segments are then only considered if they feature the same sign. With these restrictions, we obtain a dataset

of 828 LWP-tendencies and 783 N -tendencies.

We process these datasets largely in the same way as described in detail in reference [32, Section 3]. Here we only mention adaptations to the technical parameters mentioned therein. Instead of a 50%-50% split of the dataset into training and validation data, we use a smaller fraction of training data (33%) to ensure good validation. To obtain an ensemble of 5 emulated surfaces for v_{LWP} and v_{N} , we do not restrict the fraction of the training data to be used for individual ensemble members.

Quantification and uncertainty of LWP adjustment values in steady state

As a result of our interpolation technique, we obtain a mean emulator surface $v(N, \text{LWP})$, to which individual emulator ensemble members contribute according to their root-mean-square error (RMSE) in predicting the validation data [32, Equation 3]. The central value for the LWP adjustment is based on the zero-contour of this mean surface. For the uncertainty percentiles, we determine LWP adjustments from the zero-contours of a specific sampling of the emulator ensemble. For this sampling, we take 100 samples of each of the 5 ensemble members and then select a subset of these 500 samples, such that each ensemble member contributes proportionally to its RMSE-based weight, i.e. for the ensemble member with the lowest RMSE, all 100 samples are considered, and for the ensemble member with the highest RMSE, no samples are considered. Table S4 summarizes the uncertainty ranges obtained in this way for the LWP adjustment value.

Derivation of the adjustment equilibration timescale

To derive the adjustment equilibration timescale, we determine the time required by the entire system of LWPs to reach their respective steady states. We assume that the LWP for any N approaches its steady state $\text{LWP}_\infty(N)$ with approximately the same velocity $[\text{LWP}_{\text{ini}} - \text{LWP}_\infty(N_0)]/\tau$ controlled by the characteristic equilibration timescale $\tau = 9.6 \text{ h}$ (Figure S3), where LWP_{ini} is an initial non-steady-state LWP. Hence, the linearized exponential change in LWP yields

$$\text{LWP}(t, N) = \text{LWP}_{\text{ini}} - \frac{t}{\tau} [\text{LWP}_{\text{ini}} - \text{LWP}_\infty(N_0)], \tag{S1}$$

where $\text{LWP}_\infty(N_0)$ is the steady-state LWP for the smallest N in the non-precipitating regime, N_0 . Note that we focus on the LWPs that approach the steady state from larger

values since only those require a longer time to reach the steady state for larger N .

The steady-state LWP as a function of N is obtained by integrating and linearizing the adjustment $d \ln \text{LWP} / d \ln N$,

$$\text{LWP}_\infty(N) = \text{LWP}_\infty(N_0) \left[1 + \frac{d \ln \text{LWP}_\infty}{d \ln N} \ln \left(\frac{N}{N_0} \right) \right], \quad (\text{S2})$$

using the same constants of integration as above. Combining Equations S2 and S1, and solving for $t \equiv \tau_{\text{adj}}$, gives the adjustment equilibration timescale necessary to equilibrate the entire system:

$$\tau_{\text{adj}} = \tau \left[1 - \frac{d \ln \text{LWP}_\infty}{d \ln N} \ln \left(\frac{N_2}{N_0} \right) \frac{\text{LWP}_\infty(N_0)}{\text{LWP}_{\text{ini}} - \text{LWP}_\infty(N_0)} \right],$$

where $N = N_2$ is the largest droplet concentration in the considered non-precipitating regime, resulting in the longest time to equilibrate the LWP. With $N_0 = 107 \text{ cm}^{-3}$, $N_2 = 390 \text{ cm}^{-3}$ and $\text{LWP}_\infty(N_0) = 89 \text{ g m}^{-2}$ in the smallest (index 0) and largest (index 2) N -bin, and $d \ln \text{LWP}_\infty / d \ln N = -0.64$, we obtain best fitting results for τ_{adj} when assuming $\text{LWP}_{\text{ini}} = 159 \text{ g m}^{-2}$, which amounts to the 78th percentile of LWPs in the N_2 -bin. These numerical values provide the adjustment equilibration timescale stated in Equation 2.

Effective evolution time of ship tracks in a shipping lane

The effective evolution time Δt_{lane} of a ship track in a shipping lane can be estimated based on Equation 2,

$$\text{adj}(\Delta t_{\text{lane}}) = -0.24 \Rightarrow \Delta t_{\text{lane}} \approx 9 \text{ h}, \quad (\text{S3})$$

where we have used the adjustment value $d \ln \text{LWP} / d \ln N = -0.24$ from reference [17].

Cloud-mediated aerosol forcing and cloud radiative effect

The cloud-mediated aerosol forcing depends on the aerosol sensitivity of the relative cloud radiative effect, rCRE, which relates downwelling short-wave radiative fluxes at

the surface, F , under clear-sky (index *clr*) and all-sky (index *all*) conditions [51],

$$\text{rCRE} = \frac{F_{\text{clr}} - F_{\text{all}}}{F_{\text{clr}}} \approx \text{CF} \cdot A_c \approx A_c \quad (\text{S4})$$

and amounts to cloud albedo A_c in fully overcast S_c with cloud fraction $\text{CF} \approx 1$. We assume that climatological cloud properties can be approximated by steady-state values. With a steady-state cloud albedo of $A_c = 0.5$ based on Figure S5, Equation 1 for the sensitivity of A_c , or rCRE, respectively, results in

$$S = \frac{1}{N} \left(\frac{1}{12} + \frac{5}{24} \frac{d \ln \text{LWP}}{d \ln N} \right). \quad (\text{S5})$$

With $d \ln \text{LWP}/d \ln N \approx -0.1$ (Equation 3), ship-track studies imply $S_{\text{ship}} \approx 0.06/N > 0$ and thus a cooling effect of anthropogenic aerosol via increased cloud brightness at almost constant LWP. In contrast, the steady-state adjustment value of $d \ln \text{LWP}_\infty/d \ln N = -0.64$ derived here as a lower bound results in $S_{\text{clim}} = -0.05/N < 0$, which indicates that aerosol-induced cloud thinning overcompensates the brightening effect at constant LWP. Ship-track studies thus overestimate the cooling effect of aerosol on S_c by up to $|(-0.05 - 0.06)/(-0.05)| = 220\% \approx 200\%$.

Supplementary figures and tables

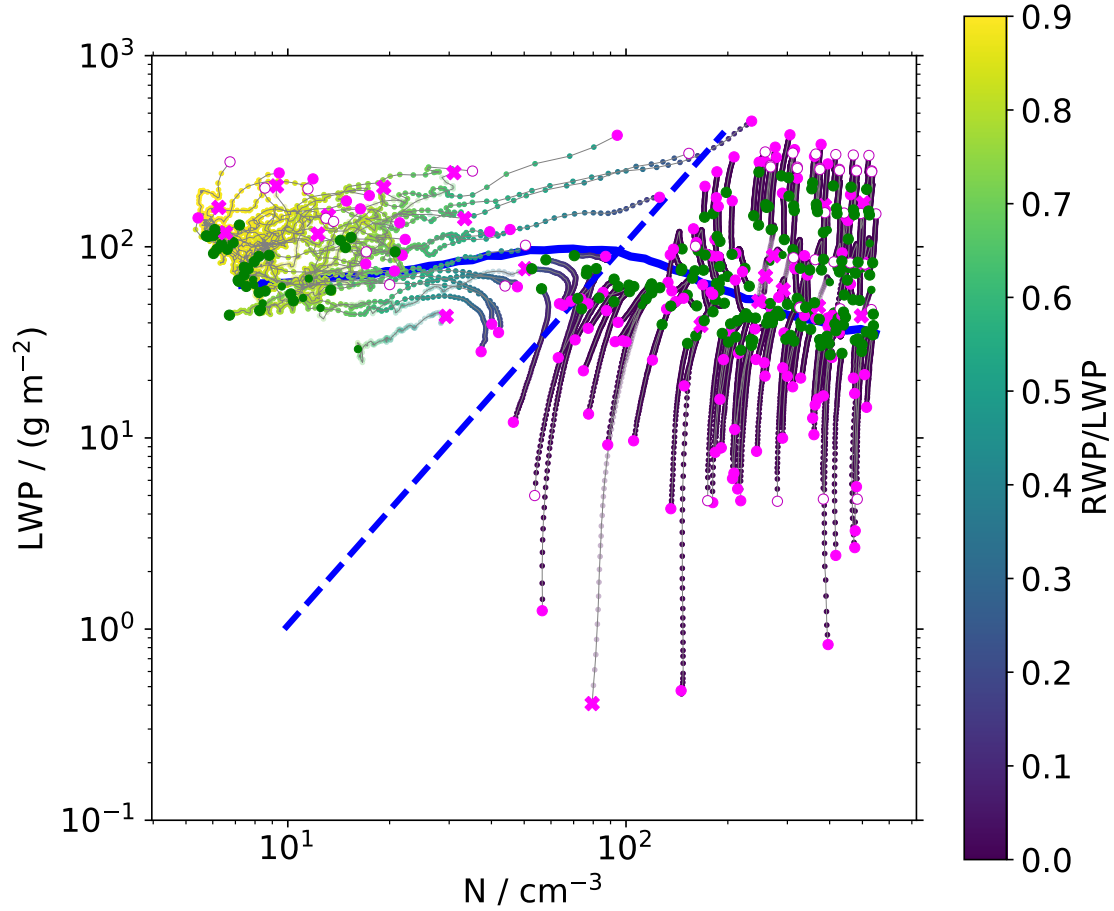


Figure S1: Dataset illustrated similar to Figure 3 (a). Trajectories in faint coloring, whose start is indicated by a cross rather than a circle, indicate runs that were excluded for this study in comparison to the dataset described in reference [32] due to their above-cloud absolute humidity being an outlier. Open magenta-colored circles indicate additional simulations only considered for deriving the flow field \vec{v} . The coloring of trajectories indicates the fractional contribution of rain water path RWP to total liquid water path LWP.

a)

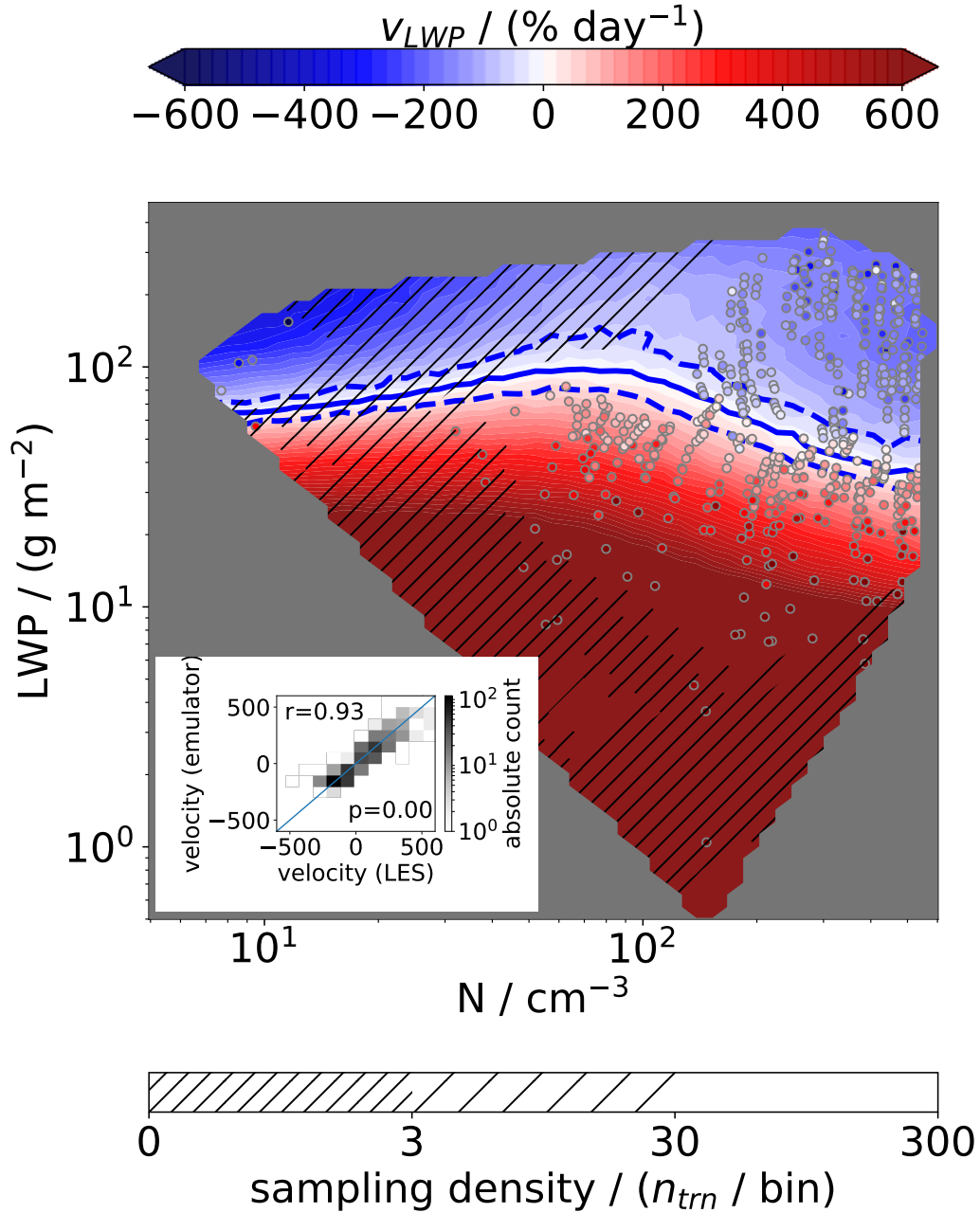
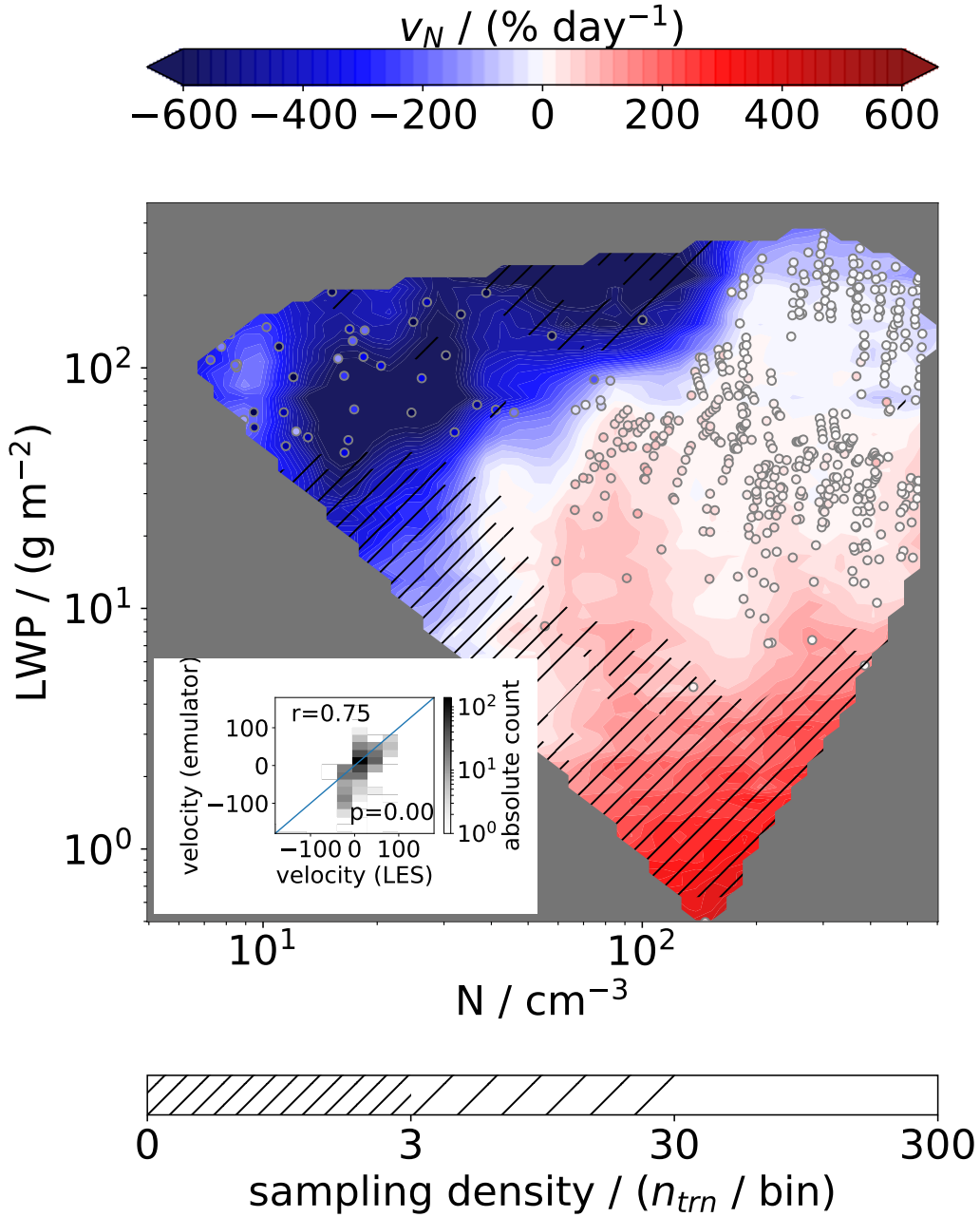


Figure S2: (See next page for continuation of figure) Emulated surfaces (average surface from an ensemble of emulators) of (a) LWP-component $v_{LWP} = d \ln LWP / dt$ and (b) N -component $v_N = d \ln N / dt$ of the flow field \vec{v} as a function of LWP and droplet number N . The dark gray area confines the convex hull of data points, within which interpolation is possible. The goodness of fit of the emulated surfaces as compared to the validation data set is illustrated by color-filled circles and by the one-to-one scatter plots in the insets, which also indicate a correlation coefficient r and a p -value for a linear relationship.

b)



(Continuation from previous page) Hatching indicates the number of training data points n_{trn} per bin, for a 10×12 binning of the N -LWP space. As discussed in reference [32], insufficient sampling is the largest source of uncertainty. Blue contour lines in (a) indicate $v_{LWP} = 0$, i.e. $LWP = LWP_\infty$, for the (dashed) 25th, (solid) 50th and (dashed) 75th percentile of a RMSE-weighted sampling from the emulator ensemble (see text). Blue curves in Figure 3 and 4 correspond to the median sampling (solid blue contour).

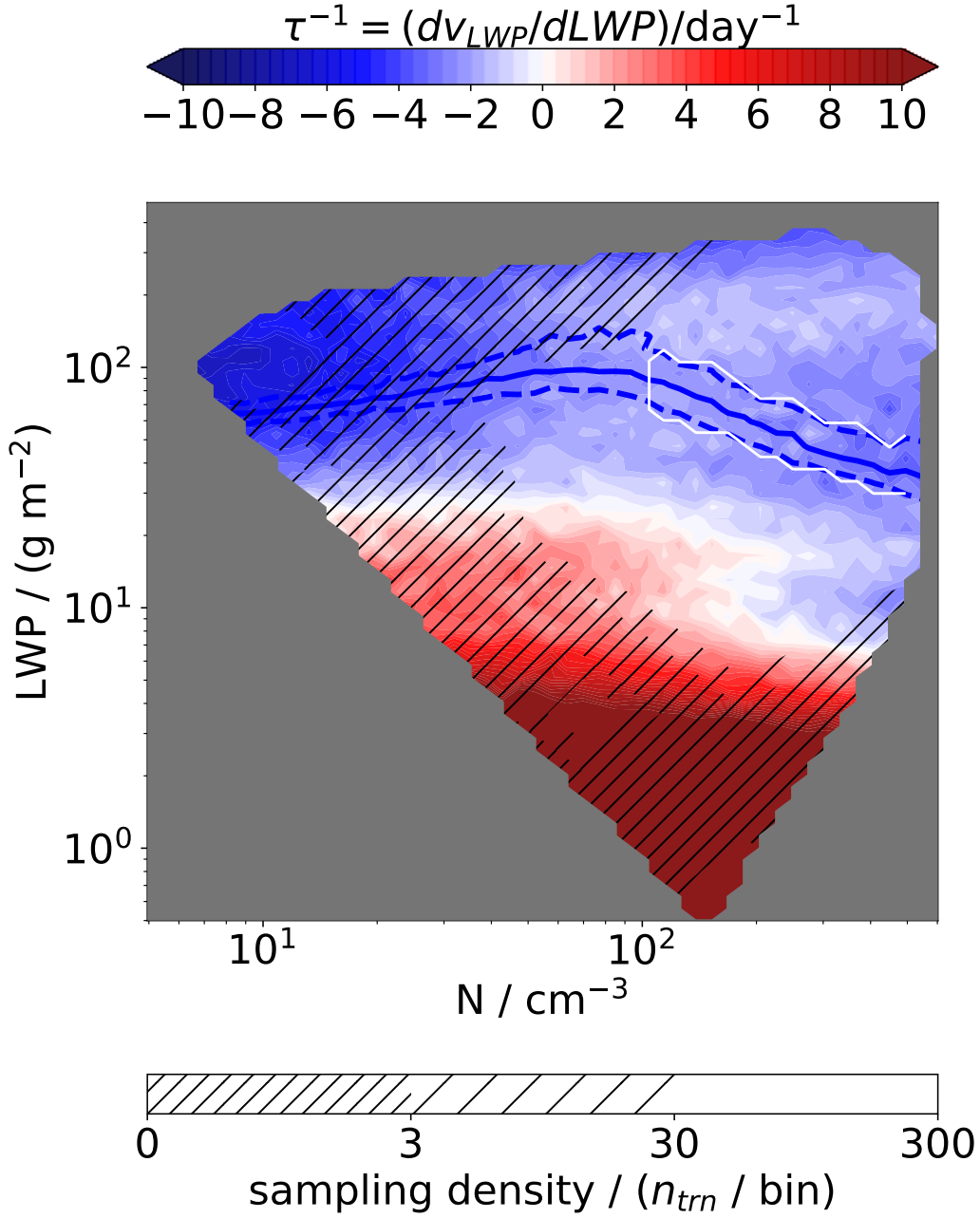


Figure S3: The characteristic equilibration timescale τ for LWP equilibration to its steady-state value LWP_{∞} is determined by $\tau^{-1} = |\partial v_{LWP}/\partial LWP|_{LWP_{\infty}}$, where the derivative (color contours) is evaluated at LWP_{∞} [36]. An average value of $\partial v_{LWP}/\partial LWP = -2.49 \text{ day}^{-1}$ within the white contour indicates a characteristic equilibration timescale of $\tau = 9.6 \text{ h}$. Sampling density as in Figure S2.

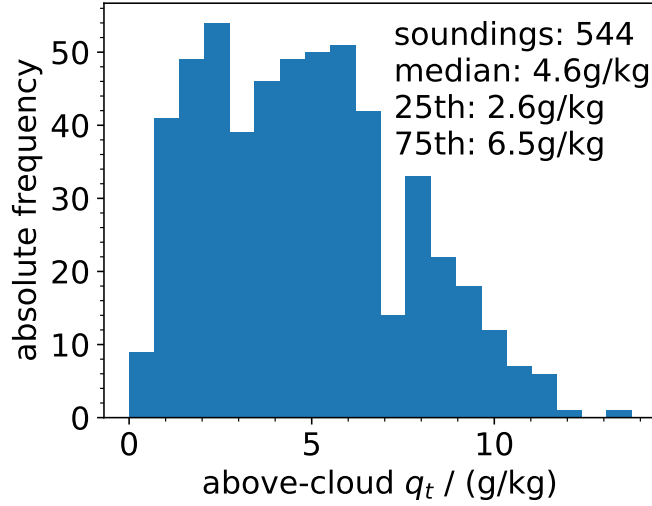


Figure S4: Climatology (1973-2020) of above-cloud mixing ratio at San Clemente Island (Station NSI 72291) in the Sc region off the coast of California. Mixing ratios are obtained at a height of $1.05z_i$, where z_i denotes the inversion height as determined from the maximum gradient in the equivalent potential temperature. Only soundings that reach saturation in the lowest 2000 m were considered. Radiosonde data kindly provided by University of Wyoming (<http://www.weather.uwyo.edu/upperair/sounding.html>).

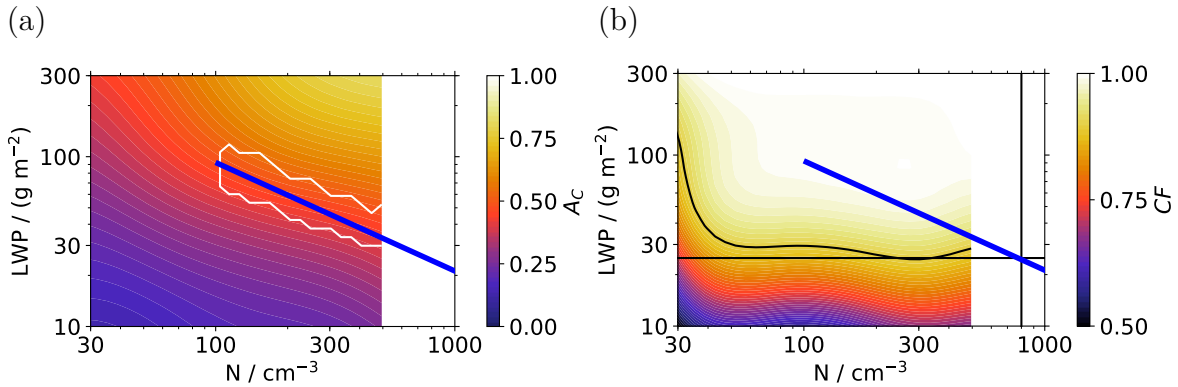


Figure S5: Emulated values for (a) cloud albedo A_c and (b) cloud fraction CF as function of cloud droplet number N and liquid-water path LWP (re-plot of results from reference [32]). Solid blue lines indicate the location of the steady-state LWP as in Figure 4. The white contour in (a) corresponds to the blue uncertainty shading in Figure 3 (b). The average cloud albedo within this white contour amounts to $A_c = 0.46$. The black contour in (b) indicates $CF = 90\%$. The horizontal and vertical black lines in (b) are conservative guides to the eye, showing that a cloud fraction reduction $CF < 90\%$ is expected for $N \approx 800 \text{ cm}^{-3}$. For larger N , no fully overcast Sc steady state exists.

	entr	prcp	reference details	data source	data type	comments
this work	-0.64	0.21	Figure 4	LES ensemble	regression	steady-state value
[8]	-0.27	0.24	Supplementary Table 1, prcp: ASTEX, FIRE1, entr: DYCOMS-RF1	LES	difference quotient	$q_t \approx 1\text{g/kg}$
[21]	-0.05	-	Table 3, HOM_FULL	LES	LWP, N (lists)	$q_t > 5\text{g/kg}$
[22]	0.11	-	Figures 4 and 8, MID-WET	LES	LWP, N (pairs)	$q_t = 5.5\text{g/kg}$
[23]	-0.12	0.24	Table 2	LES	LWP, N (pairs)	$q_t \approx 3\text{g/kg}$
[24]	0.075	0.025	Figure 4, LTS>15 K, prcp threshold: dBZe < -20	satellite	regression	no N -binning
[15]	-0.42	0.14	Figure 4 (e)	satellite	regression	-
[25]		0.03	Table 1, LTS> 18	satellite	regression	no separate fits for entr vs prcp
[26]	-0.31; -0.15	0.14	Table 1, s_{LWP} (bivariate), min and max value for entr	satellite	regression	-
[20]	-0.175	-	abstract	ship track	difference quotient	-
[14]	-0.13	0.36	Table 2, entr: closed, prcp: open	ship track	LWP, τ , r_{eff} (pairs)	-
[16]	-0.021	-	Extended Data Table 2	ship track	difference quotient	-
[17]	-0.24	-	Section 4	ship track	difference quotient	shipping lane

Table S1: Literature values used in Figure 1 and details about their derivation. Abbreviations “entr” and “prcp” refer to the entrainment- and precipitation-dominated regimes of Sc , respectively. Data source “satellite” refers to climatological satellite studies, while “ship track” refers to ship track studies from satellite. The “data type” column indicates whether adjustment information was derived as difference quotient $\Delta \ln \text{LWP} / d \ln N$ from value pairs, obtained as gradient $d \ln \text{LWP} / d \ln N$ of linear regression lines through a provided list of data points, or directly provided in one of these two forms. In one case, N was inferred from cloud optical thickness τ and effective radius r_{eff} .

horizontal wind divergence	$3.75 \times 10^{-6} \text{ s}^{-1}$
sensible heat flux	16 W m^{-2}
latent heat flux	93 W m^{-2}
aerosol surface flux	$70 \text{ cm}^{-2} \text{ s}^{-1}$
above-cloud moisture	$0.5[0.2, 2.8] \text{ g kg}^{-1}$
radiation	nocturnal

Table S2: External simulation parameters given by large-scale conditions following reference [52]. Values of above-cloud moisture refer to the median and, in brackets, the minimum and maximum value within the distribution.

mixed-layer height h (in m)	[500, 1300]
mixed-layer aerosol concentration N_a (in cm^{-3})	[30, 500]
mixed-layer liquid-water potential temperature θ_l (in K)	[284, 294]
mixed-layer moisture q_t (in g kg^{-1})	[6.5, 10.5]
inversion of liquid-water potential temperature at h $\Delta\theta_l$ (in K)	[6, 10]
inversion of moisture at h Δq_t (in g kg^{-1})	[-10, -6]

Table S3: Ranges of values that span the initial conditions of internal variables for the ensemble of LES runs used in this study, following reference [33] and assuming well-mixed initial profiles.

percentile	5th	25th	50th	75th	95th
entrainment dominated	-1.15	-0.89	-0.64	-0.55	-0.34
drizzle dominated	0.17	0.22	0.21	0.39	0.68

Table S4: Uncertainty quantification for LWP adjustment values in steady state. See text for details.

Acknowledgments

FG thanks Tom Goren and Anna Possner for helpful discussions about the interpretation of satellite literature. FG acknowledges support by The Branco Weiss Fellowship – Society in Science, administered by the ETH Zürich, and by a Veni grant of the Dutch Research Council (NWO). FH holds a visiting fellowship of the Cooperative Institute for Research in Environmental Sciences (CIRES) at the University of Colorado Boulder, and the NOAA/Earth System Research Laboratory. Jill S. Johnson and Ken S. Carslaw were supported by the Natural Environment Research Council (NERC) under

grant NE/I020059/1 (ACID-PRUF) and the UK-China Research and Innovation Partnership Fund through the Met Office Climate Science for Service Partnership (CSSP) China as part of the Newton Fund. Ken S. Carslaw is currently a Royal Society Wolfson Research Merit Award holder. This research was partially supported by the Office of Biological and Environmental Research of the U.S. Department of Energy Atmospheric System Research Program Interagency Agreement DE-SC0016275 and by an Earth's Radiation Budget grant, NOAA CPO Climate & CI #03-01-07-001. Marat Khairoutdinov graciously provided the SAM model. The University of Wyoming, Department of Atmospheric Science, is acknowledged for archiving the radiosonde data.

References

- [1] G. L. Stephens, J. Li, M. Wild, C. A. Clayson, N. Loeb, S. Kato, T. L'Ecuyer, P. W. Stackhouse, and T. Lebsack, M. and Andrews. An update on Earth's energy balance in light of the latest global observations. *Nature Geosci.*, 5(10):691–696, 2012. ISSN 1752-0908. doi: 10.1038/ngeo1580.
- [2] T. S. L'Ecuyer, Y. Hang, A. V. Matus, and Z. Wang. Reassessing the effect of cloud type on Earth's energy balance in the age of active spaceborne observations. Part I: Top of atmosphere and surface. *J. Climate*, 32(19):6197–6217, 2019. doi: 10.1175/jcli-d-18-0753.1.
- [3] O. Boucher, D. Randall, P. Artaxo, C. Bretherton, G. Feingold, P. Forster, V.-M. Kerminen, Y. Kondo, H. Liao, U. Lohmann, P. Rasch, S.K. Satheesh, S. Sherwood, B. Stevens, and X.Y. Zhang. Clouds and aerosols. In T. F. Stocker, D. Qin, G.-K. Plattner, M. Tignor, S.K. Allen, J. Boschung, A. Nauels, Y. Xia, V. Bex, and P.M. Midgley, editors, *Climate Change 2013: The Physical Science Basis. Contribution of Working Group I to IPCC AR5*. Cambridge, 2013. doi: 10.1017/CBO9781107415324.
- [4] N. Bellouin, J. Quaas, E. Gryspeerdt and S. Kinne, P. Stier, D. Watson-Parris, O. Boucher, K. S. Carslaw, M. Christensen, A.-L. Daniau, J.-L. Dufresne, G. Feingold, S. Fiedler, P. Forster, A. Gettelman, J. M. Haywood, U. Lohmann, F. Malavelle, T. Mauritsen, D. T. McCoy, G. Myhre, J. Mülmenstädt, D. Neubauer, A. Possner, M. Rugenstein, Y. Sato, M. Schulz, S. E. Schwartz, O. Sourdeval,

- T. Storelvmo, V. Toll, D. Winker, and B. Stevens. Bounding global aerosol radiative forcing of climate change. *Rev. Geophys.*, 58(e2019RG000660), 2019. doi: 1029/2019RG000660.
- [5] S. Twomey. Pollution and the planetary albedo. *Atmos. Environ.*, 8:1251–1256, 1974. doi: 10.1016/0004-6981(74)90004-3.
- [6] B. A. Albrecht. Aerosols, cloud microphysics, and fractional cloudiness. *Science*, 245:1227–1230, 1989. doi: 10.1126/science.245.4923.1227.
- [7] S. Wang, Q. Wang, and G. Feingold. Turbulence, condensation, and liquid water transport in numerically simulated nonprecipitating stratocumulus clouds. *J. Atmos. Sci.*, 60:262–278, 2003.
- [8] A. S. Ackerman, M. P. Kirkpatrick, D. E. Stevens, and O. B. Toon. The impact of humidity above stratiform clouds on indirect aerosol climate forcing. *Nature*, 432(7020):1011–4, 2004. doi: 10.1038/nature03137.
- [9] C. S. Bretherton, P. N. Blossey, and J. Uchida. Cloud droplet sedimentation, entrainment efficiency, and subtropical stratocumulus albedo. *Geophys. Res. Lett.*, 34(L03813), 2007.
- [10] J. D. Small, P. Y. Chuang, G. Feingold, and H. Jiang. Can aerosol decrease cloud lifetime? *Geophys. Res. Lett.*, 36(L16806), 2009.
- [11] F. Hoffmann and G. Feingold. Entrainment and mixing in stratocumulus: Effects of a new explicit subgrid-scale scheme for large-eddy simulations with particle-based microphysics. *J. Atmos. Sci.*, 76(7):1955–1973, 2019. doi: 10.1175/jas-d-18-0318.1.
- [12] B. Stevens and G. Feingold. Untangling aerosol effects on clouds and precipitation in a buffered system. *Nature*, 461:607–613, 2009. doi: 10.1038/nature08281.
- [13] J. Mülmenstädt and G. Feingold. The radiative forcing of aerosol-cloud interactions in liquid clouds: wrestling and embracing uncertainty. *Current Climate Change Reports*, 4(1):23–40, 2018. doi: doi.org/10.1007/s40641-018-0089-y.
- [14] M. W. Christensen and G. L. Stephens. Microphysical and macrophysical responses of marine stratocumulus polluted by underlying ships: evidence of cloud deepening. *J. Geophys. Res.*, 116(D03201), 2011.

- [15] E. Gryspeerdt, T. Goren, O. Sourdeval, J. Quaas, J. Mülmenstädt, S. Dipu, C. Unglaub, A. Gettelman, and M. Christensen. Constraining the aerosol influence on cloud liquid water path. *Atmos. Chem. Phys.*, 19:5331–5347, 2019.
- [16] V. Toll, M. Christensen, J. Quaas, and N. Bellouin. Weak average liquid-cloud-water response to anthropogenic aerosols. *Nature*, 572:51–, 2019.
- [17] M. S. Diamond, H. M. Director, R. Eastman, A. Possner, and R. Wood. Substantial cloud brightening from shipping in subtropical low clouds. *AGU Advances*, 1 (e2019AV000111), 2020. doi: 10.1029/2019AV000111.
- [18] S. Platnick and S. Twomey. Determining the susceptibility of cloud albedo to changes in droplet concentration with the advanced very high resolution radiometer. *J. Appl. Meteor.*, 33:334 – 347, 1994.
- [19] R. Boers and R. M. Mitchell. Absorption feedback in stratocumulus clouds influence on cloud top albedo. *Tellus A: Dynamic Meteorology and Oceanography*, 46 (3):229–241, Jan 1994. doi: 10.3402/tellusa.v46i3.15476.
- [20] J. A. Coakley Jr. and C. D. Walsh. Limits to aerosol indirect radiative effect derived from observations of ship tracks. *J. Atmos. Sci.*, 59:668–680, 2002.
- [21] A. A. Hill, G. Feingold, and H. Jiang. The influence of entrainment and mixing assumption on aerosol–cloud interactions in marine stratocumulus. *J. Atmos. Sci.*, 66(5):1450–1464, 2009. ISSN 1520-0469. doi: 10.1175/2008jas2909.1.
- [22] S. S. Lee, J. E. Penner, and S. M. Saleeby. Aerosol effects on liquid-water path of thin stratocumulus clouds. *J. Geophys. Res.*, 114(D07204), 2009.
- [23] H. Wang, P. J. Rasch, and G. Feingold. Manipulating marine stratocumulus cloud amount and albedo: a process-modelling study of aerosol-cloud-precipitation interactions in response to injection of cloud condensation nuclei. *Atmos. Chem. Phys.*, 11(9):4237–4249, 2011. ISSN 1680-7324. doi: 10.5194/acp-11-4237-2011.
- [24] T. Michibata, K. Suzuki, Y. Sato, and T. Takemura. The source of discrepancies in aerosol–cloud–precipitation interactions between gcm and a-train retrievals. *Atmos. Chem. Phys.*, 16(23):15413–15424, 2016. doi: 10.5194/acp-16-15413-2016.

- [25] D. Rosenfeld, Y. Zhu, M. Wang, Y. Zheng, T. Goren, and S. Yu. Aerosol-driven droplet concentrations dominate coverage and water of oceanic low-level clouds. *Science*, 363(6427):eaav0566, 2019. ISSN 1095-9203. doi: 10.1126/science.aav0566.
- [26] A. Possner, R. Eastman, F. Bender, and F. Glassmeier. Deconvolution of boundary layer depth and aerosol constraints on cloud water path in subtropical stratocumuli. *Atmos. Chem. Phys. Discuss.*, 2019. doi: 10.5194/acp-2019-833.
- [27] D. C. Leon, Z. Wang, and D. Liu. Climatology of drizzle in marine boundary layer clouds based on 1 year of data from cloudsat and cloud-aerosol lidar and infrared pathfinder satellite observations (CALIPSO). *J. Geophys. Res.*, 113(D00A14), 2008. doi: 10.1029/2008JD009835.
- [28] H. Xue, G. Feingold, and B. Stevens. Aerosol effects on clouds, precipitation, and the organization of shallow cumulus convection. *J. Atmos. Sci.*, 65(2):392–406, 2008. doi: 10.1175/2007jas2428.1.
- [29] Yi-Chun Chen, M. W. Christensen, G. L. Stephens, and J. H. Seinfeld. Satellite-based estimate of global aerosol-cloud radiative forcing by marine warm clouds. *Nature Geosci.*, 7:643–646, 2014.
- [30] F. A.-M. Bender, L. Frey, D. T. McCoy, D. P. Grosvenor, and J. K. Mohrmann. Assessment of aerosol-cloud-radiation correlations in satellite observations, climate models and reanalysis. *Clim. Dyn.*, 52:4371–4392, 2019.
- [31] J.-L. Brenguier, H. Pawlowska, and L. Schüller. Cloud microphysical and radiative properties for parameterization and satellite monitoring of the indirect effect of aerosol on climate. *J. Geophys. Res.*, 2003.
- [32] F. Glassmeier, F. Hoffmann, J. S. Johnson, T. Yamaguchi, K. S. Carslaw, and G. Feingold. An emulator approach to stratocumulus susceptibility. *Atmos. Chem. Phys.*, 19:10191–10203, 2019. doi: 10.5194/acp-19-10191-2019.
- [33] G. Feingold, A. McComiskey, T. Yamaguchi, J. S. Johnson, K. S. Carslaw, and K. S. Schmidt. New approaches to quantifying aerosol influence on the cloud radiative effect. *Proc. Natl. Acad. Sci. USA*, 113(21):5812–5819, 2016. doi: 10.1073/pnas.1514035112.

- [34] F. Hoffmann, F. Glassmeier, T. Yamaguchi, and G. Feingold. Liquid water path steady states in stratocumulus: Insights from process-level emulation and mixed-layer theory. *J. Atmos. Sci.*, 2020. doi: <https://doi.org/10.1175/JAS-D-19-0241.1>.
- [35] D. Rosenfeld and G. Gutman. Retrieving microphysical properties near the tops of potential rain clouds by multispectral analysis of AVHRR data. *Atmos. Res.*, 34:259–283, 1994.
- [36] S. H. Strogatz. *Nonlinear dynamics and chaos*. Addison-Wesley, 1994.
- [37] W. H. Schubert, J. S. Wakefield, W. J. Steiner, and S. K. Cox. Marine stratocumulus convection. Part II: horizontally inhomogeneous solutions. *J. Atmos. Sci.*, 36:1308–1324, 1979.
- [38] I. Sandu and B. Stevens. On the factors modulating the stratocumulus to cumulus transitions. *J. Atmos. Sci.*, 68(9):1865–1881, 2011. doi: 10.1175/2011jas3614.1.
- [39] B. Stevens. Bulk boundary-layer concepts for simplified models of tropical dynamics. *Theor. Comput. Fluid. Dyn.*, 20(5-6):279–304, 2006. doi: 10.1007/s00162-006-0032-z.
- [40] C. S. Bretherton, J. Uchida, and T. N. Blossey. Slow manifolds and multiple equilibria in stratocumulus-capped boundary layers. *J. Adv. Model. Earth Syst.*, 2(14):20, 2010. doi: 10.3894/JAMES.2010.2.14.
- [41] R. Wood. Stratocumulus clouds. *Mon. Wea. Rev.*, 140(8):2373–2423, 2012. doi: 10.1175/mwr-d-11-00121.1.
- [42] F. Glassmeier and U. Lohmann. Precipitation susceptibility and aerosol buffering of warm and mixed-phase orographic clouds in idealized simulations. *J. Atmos. Sci.*, 75(4):1173–1194, 2018. doi: 10.1175/JAS-D-17-0254.1.
- [43] P. Zhu, C. S. Bretherton, M. Koehler, A. Cheng, A. Chlond, Q. Geng, P. Austin, J.-C. Golaz, G. Lenderink, A. Lock, and B. Stevens. Intercomparison and interpretation of single-column model simulations of a nocturnal stratocumulus-topped marine boundary layer. *Mon. Wea. Rev.*, 133:2741–2758, 2005.

- [44] M. W. Christensen, K. Suzuki, B. Zambri, and G. L. Stephens. Ship track observations of a reduced shortwave aerosol indirect effect in mixed-phase clouds. *Geophys. Res. Lett.*, 4(6970–6977), 2014.
- [45] P. A. Durkee, R. E. Chartier, A. Brown, W. J. Trehubenko, S. D. Rogerson, C. Skupniewicz, and K. E. Nielsen. Composite ship track characteristics. *J. Atmos. Sci.*, 57:2542–2553, 2000.
- [46] T. Goren, J. Kazil, F. Hoffmann, T. Yamaguchi, and G. Feingold. Anthropogenic air pollution delays marine stratocumulus break-up to open-cells. *Geophys. Res. Lett.*, 46:14135–14144, 2019. doi: 10.1029/2019gl085412.
- [47] K. S. Carslaw, L. A. Lee, C. L. Reddington, K. J. Pringle, A. Rap, P. M. Forster, G. W. Mann, D. V. Spracklen, M. T. Woodhouse, L. A. Regayre, and J. R. Pierce. Large contribution of natural aerosols to uncertainty in indirect forcing. *Nature*, 503:67–71, 2013. doi: 10.1038/nature12674.
- [48] D. Fu, L. Di Girolamo, L. Liang, and G. Zhao. Regional biases in MODIS marine liquid water cloud drop effective radius deduced through fusion with MISR. *J. Geophys. Res. Atmos.*, 124:13182–13196, 2019. doi: 10.1029/2019JD031063.
- [49] F. F. Malavelle, J. M. Haywood, A. Jones, A. Gettelman, L. Clarisse, S. Bauduin, R. P. Allan, I. H. H. Karset, J. E. Kristjánsson, L. Oreopoulos, N. Cho, D. Lee, N. Bellouin, O. Boucher, D. P. Grosvenor, K. S. Carslaw, S. Dhomse, G. W. Mann, A. Schmidt, H. Coe, M. E. Hartley, M. Dalvi, A. A. Hill, B. T. Johnson, C. E. Johnson, J. R. Knight, F. M. O’Connor, D. G. Partridge, P. Stier, G. Myhre, S. Platnick, G. L. Stephens, H. Takahashi, and T. Thordarson. Strong constraints on aerosol–cloud interactions from volcanic eruptions. *Nature*, 546(7659):485–491, 2017. doi: 10.1038/nature22974.
- [50] R. Wood, T. Ackerman, P. Rasch, and K. Wanser. Could geoengineering research help answer one of the biggest questions in climate science? *Earth’s Future*, 5: 659–663, 2017.
- [51] Y. Xie and Y. Liu. A new approach for simultaneously retrieving cloud albedo and cloud fraction from surface-based shortwave radiation measurements. *Environ. Res. Lett.*, 8(4):044023, 2013. doi: 10.1088/1748-9326/8/4/044023.

- [52] A. S. Ackerman, M. C. vanZanten, B. Stevens, V. Savic-Jovicic, C. S. Bretherton, A. Chlond, J.-C. Golaz, H. Jiang, M. Khairoutdinov, S. K. Krueger, D. C. Lewellen, A. Lock, C.-H. Moeng, K. Nakamura, M. D. Petters, J. R. Snider, S. Weinbrecht, and M. Zulauf. Large-eddy simulations of a drizzling, stratocumulus-topped marine boundary layer. *Mon. Weather Rev.*, 137(3):1083–1110, 2009. doi: 10.1175/2008mwr2582.1.